Plant Physiology and Biochemistry 169 (2021) 171–182

Contents lists available at ScienceDirect

Plant Physiology and Biochemistry

journal homepage: www.elsevier.com/locate/plaphy

A molecular dynamics-guided mutagenesis identifies two aspartic acid residues involved in the pH-dependent activity of OG-OXIDASE 1

Anna Scortica [a], Matteo Capone [b], Daniele Narzi [b,**], Mario Frezzini [c], Valentina Scafati [a], Moira Giovannoni [a], Francesco Angelucci [a], Leonardo Guidoni [b], Benedetta Mattei [a,*], Manuel Benedetti [a]

[a] Dept. of Life, Health and Environmental Sciences, University of L'Aquila, 67100, L'Aquila, Italy
[b] Dept. of Physical and Chemical Sciences, University of L'Aquila, 67100, L'Aquila, Italy
[c] Dept. of Information Engineering, Computer Science and Mathematics, University of L'Aquila, 67100, L'Aquila, Italy

ARTICLE INFO

Keywords:
ABTS-HRP coupled Assay
pH-dependent activity
Molecular dynamics
OGs
OGOX
Plant defense
Site-directed mutagenesis

ABSTRACT

During the infection, plant cells secrete different OG-oxidase (OGOX) paralogs, defense flavoproteins that oxidize the oligogalacturonides (OGs), homogalacturonan fragments released from the plant cell wall that act as Damage Associated Molecular Patterns. OGOX-mediated oxidation inactivates their elicitor nature, but on the other hand makes OGs less hydrolysable by microbial endo-polygalacturonases (PGs). Among the different plant defense responses, apoplastic alkalinization can further reduce the degrading potential of PGs by boosting the oxidizing activity of OGOXs. Accordingly, the different OGOXs so far characterized showed an optimal activity at pH values greater than 8. Here, an approach of molecular dynamics (MD)-guided mutagenesis succeeded in identifying the amino acids responsible for the pH dependent activity of OGOX1 from *Arabidopsis thaliana*. MD simulations indicated that in alkaline conditions (pH 8.5), the residues Asp325 and Asp344 are engaged in the formation of two salt bridges with Arg327 and Lys415, respectively, at the rim of enzyme active site. According to MD analysis, the presence of such ionic bonds modulates the size and flexibility of the cavity used to accommodate the OGs, in turn affecting the activity of OGOX1. Based on functional properties of the site-directed mutants OGOX1.D325A and OGOX.D344A, we demonstrated that Asp325 and Asp344 are major determinants of the alkaline-dependent activity of OGOX1.

1. Introduction

The plant cell wall is a strong, although extensible, polysaccharide-based structure that surrounds the plasma membrane, conferring shape, structural support and protection towards both abiotic and biotic stresses. As the first cellular compartment which encounters environmental signals, the cell wall is actively involved in perception, transduction, and response to external stimuli. During infection, phytopathogens secrete a wide array of degrading enzymes that hydrolyse the different polysaccharides of the plant cell wall, opening a breach in such barrier and allowing the colonization of the tissue (Benedetti et al., 2019). Cell wall fragments released from the enzymatic hydrolysis of pectin, cellulose and certain types of hemicellulose possess elicitor activity and alert plant of the presence of invading microbes, thereby acting as Damage Associated Molecular Patterns (DAMPs) (Hou et al., 2019). The best-known DAMPs are cell wall fragments released from the enzymatic hydrolysis of homogalacturonan and amorphous region of cellulose, namely oligogalacturonides (OGs) and cellodextrins (CDs) (Pontiggia et al., 2020). Recently, the identification of several berberine-bridge like enzymes (BBE-ls) from *Arabidopsis thaliana* as specific FAD-dependent oxidases of OGs and CDs opened the way to novel insights in plant immunity (Benedetti et al., 2018; Locci et al., 2019). OG-oxidases (OGOXs) oxidize the D-galacturonic acid unit at the reducing end of each OG oligomer into galactaric acid by concomitantly releasing H_2O_2 (Pontiggia et al., 2020) (Fig. S1). The oxidized OGs (oxOGs) lose their capability of inducing plant defences in favor of an increased recalcitrance to the enzymatic hydrolysis against fungal endo-polygalacturonases (Benedetti et al., 2018), pointing to OGOX enzymes as defence proteins hindering the degrading action of microbial

* Corresponding author. Dept. of Life, Health and Environmental Sciences, University of L'Aquila, L'Aquila, Italy.
** Corresponding author. Dept. of Physical and Chemical Sciences, University of L'Aquila, L'Aquila, Italy.
E-mail addresses: daniele.narzi@univaq.it (D. Narzi), mariabenedetta.mattei@univaq.it (B. Mattei).

https://doi.org/10.1016/j.plaphy.2021.11.011
Received 16 August 2021; Received in revised form 19 October 2021; Accepted 10 November 2021
Available online 12 November 2021

Abbreviation

ABTS	2,2′-azino-bis(3-ethylbenzothiazoline-6-sulfonic acid)
BBE	Berberine Bridge Enzyme [(S)-reticuline:oxygen oxidoreductase, EC number: 1.21.3.3]
BBE-l:	Berberine Bridge Enzyme Like
CD	cellodextrin
CELLOX	Cellodextrin oxidase (cellodextrin:oxygen oxidoreductase, EC number: 1.21.3.3)
DAMPs	Damage Associated Molecular Patterns
DP	degree of polymerization
HIC	Hydrophobic Interaction Chromatography
HRP	Horseradish Peroxidase type VI-A (phenolic donor: hydrogen-peroxide oxidoreductase, EC number: 1.11.1.7)
MD	Molecular Dynamics
OG	oligogalacturonide
OGOX	Oligogalacturonide oxidase (oligogalacturonide:oxygen oxidoreductase, EC number: 1.21.3.3)
OxOG	oxidized oligalacturonide
PG	Endo-polygalacturonase (poly-α-1,4-galacturonide glycanohydrolase, EC number: 3.2.1.15)

pectinases (Fig. 1). It is worth noting that the enzymatic degradation of OGs in the presence of OGOX1 generates oxidized-trimers and -dimers which cannot be further hydrolysed by the endo-polygalacturonases into the conventional end products di- and mono-galacturonic acid, thus impeding their efficient assimilation by the fungus, and that transgenic Arabidopsis plants overexpressing OGOX1 are more resistant to *Botrytis cinerea* (Benedetti et al., 2018). On the other hand, the role of H_2O_2 released upon OG oxidation in pathogen defence and signalling is still under investigation. In *Arabidopsis thaliana*, BBE-l proteins constitute a family of 28 members (i.e., BBE1-28) characterized by different substrate specificities but only four of them displayed a proven OG-oxidizing activity, i.e., OGOX1 (AT4G20830/BBE19-20), OGOX2 (AT4G20840/BBE21), OGOX3 (AT1G11770/BBE2) and OGOX4 (AT1G01980/BBE1) (Benedetti et al., 2018). OGOX1 is encoded by the gene AT4G20830 and exists in two different isoforms as obtained by alternative splicing of the same transcript; the longer isoform (AT4G20830.1/BBE19) is localized in the lipid rafts by a C-terminal GPI-anchor like motif (Borner et al., 2005; Elortza et al., 2006) whereas the shorter isoform (AT4G20830.2/BBE20) is extracellular and performs its function in the apoplast (Benedetti et al., 2018) (Fig. 1). Although OGOX1 is a specific oxidase of homogalacturonan fragments with a degree of polymerization higher than two (i.e., dimer/digalacturonic acid), the enzyme showed the highest oxidizing activity from the heptamer onwards. All OGOX enzymes are characterized by a peculiar pH-dependent activity with a pH-optimum ranging from 8 (OGOX3-4) to 10 (OGOX1-2) (Benedetti et al., 2019). The evolutionary advantage of such an alkaline pH range for optimal enzyme activity could be related to the alkalinization process that occurs in the apoplast during pathogenesis (Moroz et al., 2017) (Fig. 1). Extracellular alkalinization is considered as one of the earliest defence responses to biotic stress (Felle, 2001); the apoplastic pH may vary among tissues but it is always acidic under rest condition, with values between pH 5 and 6; however, it can increase up to 2 units upon pathogen exposure (Klarzynski et al., 2000; Moroz et al., 2017). The plasma membrane (PM) H + -ATPases are responsible for creating and maintaining a negative membrane potential and transmembrane pH gradient, and dynamic phosphorylation of specific amino acid residues rapidly regulates proton pump activity in response to external and internal stimuli. In *Arabidopsis thaliana*, OGs induce phosphorylation of the 2 p.m. H + -ATPases AHA1 and AHA2 at the conserved residue Ser899 (Mattei et al., 2016; Nuhse et al., 2007), a modification that has been reported to inhibit proton transport (Haruta et al., 2014), and is thought to lead to extracellular alkalinization induced by elicitors.

Structural data already available for other BBE-l members from *A. thaliana* such as BBE13 and BBE15, i.e., here referred to as Monolignol Oxidase 1 and 2, respectively (Daniel et al., 2015, 2016), could be exploited to identify motifs and amino acids crucial for oxidase activity and to pinpoint putative residues of OGOX1 responsible for specificity towards OGs. However, most of these structural considerations on OGOX1 are based on prediction models since structural as well as structure-function analyses are still missing for OGOX enzymes.

In the present study, a novel approach of MD simulations was employed to identify the amino acids responsible for the increased activity of OGOX1 at alkaline pH. The role of the amino acids pinpointed by MD analysis was validated by alanine scanning mutagenesis using a recombinant OGOX1 from *Pichia pastoris*. Here, all the analysis on OGOX1 will be referred to the shorter isoform, i.e., BBE20, whereas the amino acid numbering will start from the first amino acid of the mature protein.

2. Materials and methods

2.1. Construction of the synthetic gene encoding OGOX1 by bioinformatic tools

The sequence encoding the splice variant 2 of OGOX1 from *Arabidopsis thaliana* (AT4G20830.2, aa: 31–540) was codon-optimized according to the codon usage of *Pichia pastoris* using the software OPTIMZER (http://genomes.urv.es/OPTIMIZER/) (Puigbò et al., 2007). The putative plant signal peptide of OGOX1 was identified by using the

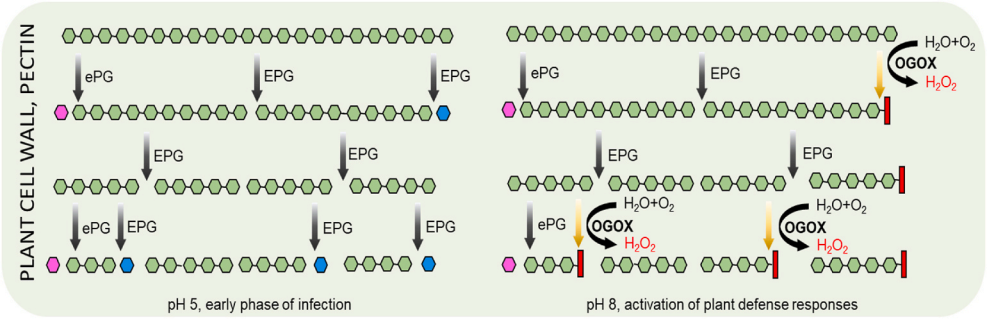

Fig. 1. Role of OGOX in plant defense. Degradation of homogalacturonan by microbial exo- (ePG) and endo-polygalacturonases (EPG) alone in the early phase of infection (*left*), and in the presence of OGOX upon activation of plant defense response (*right*). Galacturonic acid units released from the non-reducing and reducing ends of each fragment are colored in pink and turquoise, respectively. Reactants (H_2O, O_2) and products (H_2O_2) of the reaction catalyzed by OGOX are also reported. Extracellular alkalinization may favor the reaction catalyzed by OGOX enzymes due to their high pH activity optimum. The oxidized end (OE) is represented by a red rectangle. This figure is partially readapted from Benedetti et al., (2019). (For interpretation of the references to color in this figure legend, the reader is referred to the Web version of this article.)

SignalP-5.0 server (http://www.cbs.dtu.dk/services/SignalP/) (Almagro Armenteros et al., 2019) and excluded from such manipulation. The codon-optimized sequences encoding the 6x histidine tag (HHHHHH) and TEV protease cleavage site (ENLYFQG) interconnected by the dipeptide GS were added in frame to the 5^{I} end of the gene sequence encoding the mature OGOX1 splice variant 2. The sequences encoding the restriction sites *Pst*I and *Xba*I were added at the 5^{I} and 3^{I} ends of such sequence and used to clone the synthetic gene in pPICZαB (Invitrogen, San Diego, CA) in frame with the sequence encoding the yeast α factor for secretion in the culture medium. The entire sequence was synthesized by Genescript (https://www.genscript.com/). The tagged version of OGOX1 here described will be referred to as H-OGOX1 throughout the manuscript.

2.2. Heterologous expression of H-OGOX1 in Pichia pastoris

The construct pPICZαB/H-OGOX1 was transformed in *Escherichia coli* DH5α, here used as a host for plasmid propagation. After amplification, the construct was linearized by *Sac*I and transformed in *P. pastoris* by electroporation according to (Wu and Letchworth, 2004). Primary transformants were selected on solid YPDS medium [1% (w/v) yeast extract, 2% (w/v) peptone, 2% (w/v) dextrose, 1 M Sorbitol] using zeocin as selection marker (100 μg mL^{-1}). Integration of the gene into the *P. pastoris* genome was confirmed by colony PCR using 5′AOX1-F (5′-GACTGGTCCAATTGACAAGC-3′) and 3′AOX1-R (5′-CGAAATGGC ATTCTGACATGG-3′) primers according to Easy Select™ Pichia Expression Kit instructions (Invitrogen, Carlsbad, CA, USA). Multicopy transformants were positively selected by growing primary transformants on solid YPD medium [1% (w/v) yeast extract, 2% (w/v) peptone, 2% (w/v) dextrose] at increasing zeocin concentration (from 300 up to 1000 μg mL^{-1}). For protein expression at small scale, twenty colonies of multicopy *P. pastoris* transformants were inoculated in 5 mL of YPD medium supplemented with 200 μg mL^{-1} zeocin and incubated at 28 °C in a rotary shaker at 180 rpm for 72h. After reaching the stationary growth phase, the culture was centrifuged and the pellet resuspended in 1.5 mL of Buffered Minimal Medium [BMM; 0.1 M K-phosphate (pH 6.0), 1.34% (w/v) YNB, 4×10^{-5}% (w/v) biotin and 0.5% (v/v) methanol] to induce the expression of H-OGOX1 and the growth prolonged for additional 48 h. The filtrates from 48 h-grown cultures were centrifuged and the filtrates evaluated by SDS-PAGE and immunodecoration analysis by using a monoclonal anti-HIS antibody (AbHis, Bio-rad) to detect the expression of H-OGOX1. Activity of H-OGOX1 in raw extracts was spectrophotometrically determined using the orange-xylenol assay using OGs as substrate in accordance with (Benedetti et al., 2018).

2.3. Purification of H-OGOX1

At large scale, the purification of H-OGOX1 was achieved from 1 L of 48h-grown BMM culture. After cell removal by centrifugation (2500×*g*, 5 min), the culture filtrate was filtered with a sterile Polyether Sulfone (PES) filter (cut-off 0.2 μm) and concentrated by using a modular tangential flow system (Vivaflow® 200, cut-off: 30 kDa). Purification was performed by using two consecutive hydrophobic interaction chromatographies (HIC) carried out at two different pH values (pH 5.5 and 7.5) using HiTrap Phenyl FF-High Sub columns (GE Healthcare). Before HIC, $(NH_4)_2SO_4$ was added to the filtrate at a final concentration of 2 M; the sample was then loaded on a 5 mL of HiTrap Phenyl FF column pre-equilibrated with 50 mM NaAc (pH 5.5) and 2M $(NH_4)_2SO_4$. Elution was performed by a linear gradient using a buffer consituted of 50 mM NaAc (pH 5.5) and the eluted fractions were visual analyzed by SDS-PAGE analysis. Fractions containing the highest amount of H-OGOX1 were pooled and loaded on a 1 mL of HiTrap Phenyl FF (High Sub) pre-equilibrated with 50 mM Tris-HCl (pH 7.5) and 2 M $(NH_4)_2SO_4$. Elution was performed by a linear gradient using a buffer constituted of 50 mM Tris-HCl (pH 7.5). Eluted fractions were visual-analyzed by SDS-PAGE/Coomassie blue staining in order to assess the purity of the protein. Eluted fractions from 13 to 15 were pooled and used for enzymatic assays and steady-state kinetic analysis. Quantification of the amount of OGOX1 in eluted fractions was performed in Coomassie-stained gel by comparing the intensity of specific bands with a standard curve of BSA (Quantity-One software, Biorad).

2.4. 3D-structural model of OGOX1

The 3D-structural model of the short OGOX1 isoform was obtained through the SWISS– MODEL software (https://swissmodel.expasy.org) using the amino acid sequence of the mature protein (i.e., without the predicted signal peptide; the first amino acid corresponds to Q31 of the entire protein) and the crystal structure of the Monolignol Oxidase 2 (PDBe:4ud8), here used as template for homology-based molecular modelling (Biasini et al., 2014). The structural figures were prepared using CCP4mg (http://www.ccp4.ac.uk/MG/references.html) (McNicholas et al., 2011) and PyMOL (https://pymol.org/2/).

2.5. Molecular dynamics analysis of OGOX1

Molecular dynamics analysis was performed by using the 3D-structural model of OGOX1 as template (*see* Paragraph 2.4 for further details). Using propKa web server (Li et al., 2005) several residues with a calculated pKa between 5 and 8.5 have been identified. Therefore, the protonation state of the residues Asp93, His145, Glu181, His249, Asp325, Asp354, Glu366, Lys404, Lys407, Asp453, His461 have been properly adapted to the different pH conditions as described in Table 1. The models include ~30.000 TIP3P (Jorgensen et al., 1983) water molecules in an octahedron box with a buffer of 1.6 nm from the protein to box. 338 water molecules were present as structural water in the Monolignol Oxidase 2 crystallographic structure and kept in the same positions. In order to achieve the electric neutrality and an extracellular concentration of 50 mM, 32 Na^{+} cations and 57 Cl^{-} anions have been added in the solvation water molecules. The protein has been modeled using Amber ff14SB (Maier et al., 2015)and the cofactor has been described by Generalized Amber Force Field (GAFF) (Wang et al., 2004). OGOX family is constituted of FAD dependent enzymes in which the cofactor is covalently bound to the protein. The FAD atomic charges for classical MD simulations have been calculated with Restrained Electrostatic Potential Method (RESP) (Bayly et al., 1993). Optimization and electrostatic potential have been performed with Gaussian16 (Frisch et al., 2016) using HF level and 6-31G* basis set. In the RESP calculation the entire FAD molecule and the residues His90 and Cys152 from the protein have been included. The two amino acids have been capped with ACE on C terminal and NME on the N-terminal on each residue, as standard procedure for RESP calculation. The charge of the backbone atoms of His90, Cys152 and all the charges of ACE and NME have been constrained to the GAFF values. Particle Mesh Ewald (PME) (Essmann et al., 1998) method has been used for the calculation of long-range electrostatic interactions with a grid spacing for the Fast Fourier Transform of 0.12 nm and a short-range cutoff of 1.0 nm. A reciprocal

Table 1
pKa and protonation states of residues differing in the two simulated models.

Residue (pKa)	pH5	pH 8.5
Asp93 (5.1)	-COOH	-COO-
His145 (6.1)	His+	His
Glu181 (5.1)	-COOH	-COO-
Asp325 (8.4)	-COOH	-COO-
Asp354 (6.2)	-COOH	-COO-
Glu366 (5.0)	-COOH	-COO-
Lys404 (7.2)	-NH3+	-NH2
Lys407 (5.5)	-NH3+	-NH2
Asp453 (5.1)	-COOH	-COO-
His461 (6.5)	His+	His

grid of 128 × 128 × 128 cells was used with 4th order B-spline interpolation. Neighbor searching has been performed every 10 steps. Bond lengths involving hydrogen atoms have been constrained to a constant value using the LINCS algorithm (Hess et al., 1997). Periodic boundary conditions on XYZ axis have been set. The two models have been optimized using steepest descent algorithm. The MD simulations have been carried on using a timestep of 2 fs at the temperature of 310K. The temperature has been kept constant using v-rescale thermostat (Bussi et al., 2007) and the Berendsen pressure bath (Berendsen et al., 1984) was used to keep the pressure constant at a value of 1 bar. Each simulation has been equilibrated for 20 in NVT ensemble with a constraint of 1000 kJmol^{-1} nm^{-2} on the position of the protein's heavy atoms. Afterwards the models have been simulated with a decreasing constraint force on the heavy-atoms from 1000 to 100 and from 100 to 10 kJmol^{-1} nm^{-2} in NPT ensemble in order to obtain a smooth relaxation of the starting homology structure. Each position restrained simulation had the duration of 20 ns. After the equilibration, the production run has a length of 1000 ns for both pH 5 and pH 8.5 simulations. MD simulations have been carried out using GROMACS package (Abraham et al., 2015; Páll et al., 2015). Further details on the reaction pocket volume analysis are reported in the section "Data Analysis" (see Paragraph 2.9).

2.6. Site-directed mutagenesis of H-OGOX1

The construct pPICZαB/H-OGOX1 was used as template for site-directed mutagenesis. The four mutants H-OGOX1.C12A, H-OGOX1.C75A, H-OGOX1.D325A and H-OGOX1.D344A were constructed by PCR using GENEART® Site-Directed Mutagenesis System (Invitrogen) in accordance with the supplier's protocol. Primers were mutagenized in accordance with the mutations to introduce within the gene sequence. The primer sequences carrying the mutations are listed in Table 2. The PCR products were transformed into *E. coli* XL10-Gold® Ultracompetent Cells (Agilent Technologies) that, in turn, were used for plasmid propagation. Before introduction in *P. pastoris*, the four different constructs were sequenced in order to verify the presence of desired mutations. Heterologous expression, purification and enzymatic characterization were performed according to the same procedures employed for H-OGOX1.

2.7. Steady-state kinetics of H-OGOX1 and site-directed variants by ABTS-HRP coupled assay

Steady-state kinetics of H-OGOX1 and site directed variants H-OGOX1.D325A and H-OGOX1.D344A were evaluated by using different concentrations of a standard OG mixture (5–400 μM) and 30 ng of each purified enzyme in a reaction volume of 0.1 mL. The OG mixture used in this work was prepared according to (Benedetti et al., 2017) and characterized by a degree of polymerization (DP) ranging from 12 to 16 with an average DP of 14 (2482 g mol^{-1}). Steady-state kinetics of H-OGOX1 was investigated using an ABTS-HRP coupled assay [0.1 mM ABTS 2, 2′-azino-bis-(3-ethylbenzothiazoline-6-sulfonic acid) and 0.05 g.L^{-1} of horseradish peroxidase type VI-A (HRP)]. ABTS and HRP were both purchased from Sigma-Aldritch (Saint Louis, USA). The OG-oxidizing activity of H-OGOX1 and site-directed variants was evaluated at pH 5.0 (50 mM NaCl and 50 mM NaAc) and pH 8.5 (50 mM NaCl and 50 mM Tris-HCl) in the presence of HRP and ABTS, and expressed as μmol of H_2O_2 released per mg of enzyme (i.e., μmol H_2O_2.mg^{-1}). The HRP-mediated oxidation of ABTS into the cationic radical ABTS^{+}• by the H_2O_2 released upon OG-oxidation was measured in continuum mode for 10 min (one time-point each 0.2 min) at 415 nm (ε415nm = 6.29 × 10^4 M^{-1} cm^{-1}) using an Infinite® M Nano200 spectrophotometer (Tecan AG, Männedorf, Switzerland). For the construction of the calibration curve, the oxidation of ABTS was measured under the same pH conditions by using different concentrations of H_2O_2 in the presence of HRP and ABTS (Cai et al., 2018). The pH-optimum of activity of pure H-OGOX1 and site-directed variants was determined by the orange-xylenol assay using 40 μM OGs and 30 ng of each purified enzyme in a reaction volume of 0.1 mL. All the enzymatic assays were performed at 25 °C, unless otherwise specified. Further details on the analysis of kinetic parameters and pH-optimum of activity are reported in the section "Data Analysis" (see Paragraph 2.9).

Table 2
Primers used to generate the four H-OGOX1 mutants. Mutated nucleotides are underlined.

H-OGOX1 VARIANT		SEQUENCE
H-OGOX1.C12A	Fw	caactctttttgaaggctttttctgataagacta
	Rv	tagtcttatcagaaaaagccttcaaaaaagagttg
H-OGOX1.C75A	Fw	ttctgctgctgttactgcttctaagactttgaac
	Rv	gttcaaagtcttagaagcagtaacagcagcagaa
H-OGOX1.D325A	Fw	atctgctttgtggtgggctaacagattgaacgcta
	Rv	tagcgttcaatctgttagcccaccacaaagcagat
H-OGOX1.D344A	Fw	tttggatagaaacttggctacttcttcttttggta
	Rv	taccaaaagaagtagccaagtttctatccaaa

2.8. Multiple protein alignment and homology tree by bioinformatic tools

Signal peptide prediction on BBE-l enzymes was carried out using the SignalP-5.0 server (http://www.cbs.dtu.dk/services/SignalP/) in order to exclude the sequence encoding the signal peptide of each protein from the alignment. Amino acid identity analysis between the short OGOX1 isoform and the other plant BBE-l members (with experimentally validated substrates) was carried out on the mature proteins using Clustal Omega (https://www.ebi.ac.uk/Tools/msa/clustalo/). Multiple amino acid alignment was generated using the Clustal Omega output for the software Multiple Align Show (http://www.bioinformatics.org/sms/multi_align.html) whereas the homology tree was generated using the amino acid sequences of mature BBE-ls as input for the software DNA-MAN (Lynnon Biosoft).

2.9. Data Analysis

For the reaction pocket volume analysis, the Epock plugin (Laurent et al., 2015) on VMD (Humphrey et al., 1996) was used. Epock plugin requires a predefined volume defined by inclusion spheres around the mass center of a residue or around an atom, and from this volume the occupation of the protein is subtracted. In order to include all the cavity volume and as less volume as possible from the protein surface, six residues from the edge of the cavity have been identified and also the atom N5 from the FAD has been selected. The six residues are: Arg235, Arg265, Gln269, Asn326, Asp344, Lys415. The inclusion sphere radius around the residues mass center is 8 Å and the radius around the N5 atom of FAD is 6 Å. Other structural analysis including, root mean square deviations, root mean square fluctuations and distances between residues have been carried out using the respective tools of the GROMACS package (Abraham et al., 2015; Páll et al., 2015).

For the evaluation of the kinetic parameters, the absorbance at 415 nm (i.e., the wavelength at which the absorption of the cationic radical ABTS^{+}• is maximal; Cai et al., 2018) from the enzymatic reactions was measured in continuum mode, subtracted to that of the control reactions (i.e., reactions with the boiled enzyme) and converted into μmol H_2O_2.mg^{-1} by interpolation with the H_2O_2-calibration curve. Each enzymatic reaction was performed in triplicate. The tangent line along the linear phase of the reaction allowed to extrapolate the initial velocity V_0 value (i.e., μmol H_2O_2.mg^{-1}.min^{-1}). Subsequently, the averaged V_0 values as obtained from the enzymatic reactions with different OG concentrations (5–400 μM) were used as input for the tool "Very Simple K_M V_{max} Tool Kit" (http://ic50.org/kmvmax.html) to determine the K_M (i.e., μM) and V_{max} parameters (i.e., μmol H_2O_2.mg^{-1}.min^{-1}). Each V_{max} value was then divided by 0.017 (1 mg of H-OGOX1 corresponds to 0.017 μmol) in order to obtain the corresponding k_{cat} value (i.e., min^{-1}).

For the evaluation of the pH-dependent activity, the μmoles of H_2O_2

generated by each H-OGOX isoform in the pH range 5.0–10.6 were evaluated at four different time-points from the linear phase of the reaction. The relative activity (%) was calculated at each pH value as [(μmol H_2O_2.mg^{-1} at pH X)/(μmol H_2O_2.mg^{-1} at pH-optimum) *100%] by obtaining a pH-dependent activity curve for each time-point tested; then, the percentage values from the four curves were averaged and the resulting means used to construct the pH-dependent activity curves shown in Fig. 7.

3. Results

3.1. Heterologous expression of H-OGOX1 in P. pastoris

Heterologous expression of OGOX1 in *P. pastoris* had been carried out previously (Benedetti et al., 2018). However, the low yield of recombinant protein (≤2 mg.L^{-1}) and its poor stability in low salt conditions limited the possibility to perform accurate enzyme kinetics. Here, we attempted to ameliorate the yield of recombinant OGOX1 by introducing two main modifications: (i) the sequence encoding the mature OGOX1 was codon-optimized according to the codon usage of *P. pastoris* and (ii) fused downstream of the sequences encoding the 6xhis tag and TEV proteolytic site (Fig. 2A). The fusion gene was cloned in the methanol-inducible vector pPICZαB in frame with the sequence encoding the α-factor signal peptide, allowing the secretion of the recombinant protein in the chemically defined medium BMM (Invitrogen, Carlsbad, CA, USA). Compared to the previous expression strategy (Benedetti et al., 2018), the use of a codon-optimized sequence allowed to reach a higher protein yield, since several multicopy transformants showed a higher plateau of expression ranging from 5 to 7 mg protein.L^{-1} (Fig. 2B). Despite H-OGOX1 was fused to the 6xhis-tag, His-affinity chromatography failed to capture the enzyme and therefore such step was excluded by the purification procedure (data not shown). The lack of the possibility of using an affinity chromatography to purify the enzyme together with the necessity of maintaining the enzyme in proper conditions of ionic strength moved us to design an alternative purification strategy consisting of two consecutive hydrophobic interaction chromatographies (HIC) performed at different pH values, i.e., 5.5 and 7.5. Thus, the ammonium sulfate employed in HIC steps maintained the stability of the enzyme, allowing to achieve a good enzyme purity (≥85%) at the end of purification procedure (Fig. 2C). Preliminary assays using xylenol-orange assay revealed that H-OGOX1 was active with a specific activity towards OGs at pH 8.5 [2.4 ± 0.2 μmol H_2O_2.mg^{-1}.min^{-1}] comparable to that displayed by the OGOX1 isoform from Benedetti et al., (2018) (Fig. 2D). H-OGOX1 was stabilized by adding salts such as $CaCl_2$ and NaCl in the reaction medium; in particular, the presence of 50 mM NaCl was highly beneficial to preserve the activity of the enzyme over time (Fig. S2).

3.2. Molecular dynamics analysis of OGOX1

The 3D-structural model of the short OGOX1 isoform was obtained by means of homology-based molecular modelling using the crystallographic structure of Monolignol Oxidase 2 from *A. thaliana* (PDB ID: 4UD8, Daniel et al., 2015) as template, with the latter showing an amino acid identity of 39.61% with the short OGOX1 isoform (Fig. S3). As expected, the structure shows the presence of an enzyme cavity required for the substrate entry. Additionally, typical features shared by most Arabidopsis BBE-l enzymes and other plant species are present in the structure (Benedetti et al., 2018; Daniel et al., 2016, 2017). In particular, two Tyr and one Lys residues (i.e., Tyr166, Tyr451 and Lys407), suggested to form a key moiety for the catalytic mechanism of Monolignol Oxidase 2 (Daniel et al., 2015), are found here in the same conformation

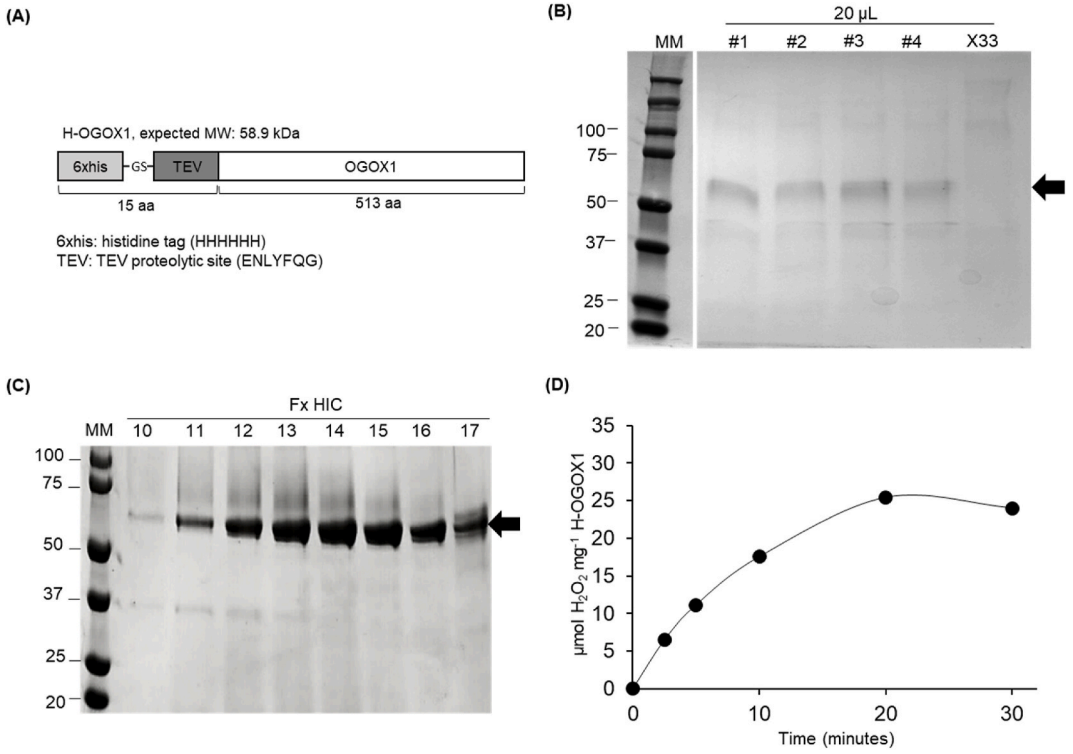

Fig. 2. Heterologous expression of H-OGOX1 in *P. pastoris*. (A) Schematic representation of his-tagged OGOX1, i.e., H-OGOX1. The amino acid sequence of OGOX1 was fused at the N-terminus to 6xhis-tag and TEV proteolytic site. (B) SDS-PAGE/Coomassie blue staining analysis of the culture filtrates from four different (#1–4) methanol-induced cultures of *P. pastoris*. Four independent multicopy transformants (#1–4) were analyzed together with the culture filtrate from *P. pastoris* X33, here used as negative control. Black arrow points to H-OGOX1. (C) SDS-PAGE/Coomassie blue staining analysis of fractions (fx) eluted from the hydrophobic interaction chromatography (HIC). Black arrow points to H-OGOX1. Molecular weight marker (MM) is also reported. (D) OG-oxidizing activity of H-OGOX1 at pH 8.5 using 0.4 mM OGs as substrate by spectrophotometric method (i.e., orange-xylenol assay).

adopted in Monolignol Oxidase 2 in the proximity of FAD. Moreover, the residue Val155, identified as gatekeeper residue of the oxygen binding pocket (Zafred et al., 2015), is also present in OGOX1. Notably, all plant BBE-l proteins acting as carbohydrate oxidases share these features (Benedetti et al., 2018). Finally, the residues covalently bound to FAD (i.e., His90 and Cys152) are also conserved in OGOX enzymes (Daniel et al., 2015, 2016) (Fig. S4).

The 3D-structural model of OGOX1 also revealed the presence of a solvent-exposed sulfur bridge between the residues Cys12 and Cys75, which is conserved among BBE-l enzymes (Fig. S4). In order to understand the effect of pH on the tuning of the catalytic features of OGOX1 at molecular level, two classical MD simulations of the OGOX1 protein have been performed considering two different pH values. From experimental measurements the highest activity of OGOX1 is around pH 10. Such a value is unlikely to occur in natural systems, therefore the selected value for the simulation in high pH conditions was set to 8.5, compatible with a stress condition in plants. As low pH, a value of 5 has been selected, being such value compatible with an apoplast pH value at physiological condition. Even though pH 8.5 does not correspond to the highest activity, a change of the catalytic properties of many folds with respect to pH 5 is expected (Benedetti et al., 2018). The two simulated models differ for the protonation state of the residues: Asp93, His145, Glu181, His249, Asp325, Asp354, Glu366, Lys404, Lys407, Asp453, His461 (Table 1). These residues have been identified by an empirical pK_a prediction server (*see* Paragraph 2.5). At pH 5, Asp93, Glu181, Asp325, Asp354, Glu366 and Asp453 have been set in their neutral form, whereas His145, His249, Lys404, Lys407 and His461 as cations. At pH 8.5 His145, His249, Lys404, Lys407 and His461 have been set in their neutral form whereas Asp93, Glu181, Asp325, Asp354, Glu366 and Asp453 as anions. The overall structural stability of the OGOX1 protein for the two simulated systems was monitored following the time evolution of different properties. The root mean square deviation (RMSD) of the backbone atoms of the protein calculated with respect to the starting positions was found to remain below 0.3 nm in both simulations (Data S1). The radius of gyration of the protein backbone was also calculated along the simulation time, finding no significant drifts in both systems (Data S2). The number of H-bond present in the two simulated models as function of time was also calculated and appears to be stable along the simulation time for both systems (Data S3). Notably, the model at pH 8.5 shows an average value of hydrogen bonds slightly larger when compared with the low pH system, thus indicating a possible higher structural stability of the protein at high pH. Overall, these analyses indicate a global stability for both models on the microsecond timescale. In order to identify possible different mobilities of the protein regions in the two simulated systems, we calculated the root mean square fluctuation (RMSF) per residue (Fig. S5). Intriguingly, two regions corresponding to the residues from 350 to 375 and from 430 to 455 were found to be more flexible in the low pH simulation with respect to the high pH simulation. Tyr451, belonging to one of the two above mentioned regions, corresponds to Tyr479 of Monolignol Oxidase 2. This residue was suggested to form with Tyr193 a key moiety for the catalytic mechanism of Monolignol Oxidase 2 (Daniel et al., 2015). Therefore, such residue should remain close to FAD in order to enable the catalytic activity of the enzyme. In this context, we monitored the distance between the oxygen atom of the side chain of Tyr451 and the nitrogen atom N5 of FAD (Fig. S6) sampled along the two simulations. Our results clearly show that at high pH the conformations of Tyr451 sampled along the MD simulations remain close to the starting one in proximity of FAD. Conversely, at low pH, the side chain of Tyr451 changes its orientation, thus losing its original conformation required for the catalytic activity of the enzyme. This observation suggests that the pH-dependent activity of OGOX1 could be related to a pH-dependent destabilization of the active site. Apart from the possible conformational changes occurring in the active site at different pH values, we focused our attention also on the interactions between key residues showing different behaviors in the two simulated systems and possibly involved in modulating the catalytic activity of OGOX1. In particular, looking at the salt bridges involving residues Asp325, Asp344, and Arg327 (Fig. 3A–C), we found some major differences between the two simulated systems. Distances between Arg327 and the two aspartic acids Asp325 and Asp344 have been calculated along the two simulated trajectories and their distribution reported in Fig. 3D. At pH 8.5, the distance between the carboxylate group of Asp325 and the guanidine group of Arg327 remains at values smaller than 5 Å, thus indicating the presence of a stable salt bridge between these two residues. The stability of such interaction results in the absence of stable interaction between Arg327 and Asp344 as evident from the respective distribution of distances lastingly larger than 6 Å. This is not the case for the simulation at low pH. Indeed, at pH 5, the distances between Asp325 and Arg327 show a broad distribution of values, most of them larger than 6 Å (Fig. 3D). On the other side, the distribution of distances between Arg327 and Asp 344 shows a pick at about 3.8 Å, thus indicating the presence of a salt bridge between these two residues, albeit not present for the whole simulation time. Indeed, as evident from the broad distribution of the Arg327-Asp344 distances at values larger than 6 Å, the interaction between these two residues is less stable along the low pH simulation with respect to the case of the Arg327-Asp325 interaction at high pH (Fig. 3D). The reason of the two distinct behaviors shown by our simulations at different pH values, resides in the different protonation state of Asp325 in the two simulated models (Table 1). The residue Asp325 has a neutral sidechain in the low pH simulation and therefore it is unable to form a salt bridge. Conversely, at high pH, the negative Asp325 residue forms a very stable salt bridge with the neighbor positive residue Arg327. From the other side, due to the lack of a stable salt bridge partner for Arg327 at pH 5, the residue that shows the most frequent interaction with Arg327 is Asp344. Due to their position in OGOX1, in the proximity of the entrance of the cavity leading to the reaction center, the different behavior shown by these residues at different pH may have implications on the catalytic activity of the enzyme. Using the cavity analysis tool Epock the volume of the cavity along the two dynamics has been tracked as described in Paragraph 2.4. As shown in Fig. 3E, a different distribution of the cavity volume was observed in the two simulations. In the low pH simulation, the cavity is characterized by a narrow fluctuation around an average value of ~3600 $Å^3$. On the contrary, at high pH, the distribution of the volumes is wider, with a maximum value corresponding to ~3900 $Å^3$. It is worth to mention that also the lowest volume values are observed in the high pH simulation, so based on our results we cannot univocally associate the low pH to the presence of a narrower cavity and the high pH to the presence of a larger cavity. Nonetheless, our simulations show a preference of the system at pH 8.5 to sample conformations characterized by a larger cavity volume with respect to the low pH simulation. In this regard, additional MD simulations starting from different initial conditions should be carried out to lead support to our observations. Overall, from this analysis, two opposite conformations have been identified from the cavity dynamics, i.e., a totally closed and an open conformation respectively shown in Fig. 3B and C. As expected, the shape of the cavity partially correlates with the conformations sampled by residues Asp325, Asp344, Arg325 and Lys415. In particular, in the high pH simulation, the presence of a salt bridge between Asp344 and Lys415 is often associated with an increased volume of the cavity, while the absence of such ionic interaction usually corresponds to a narrower cavity entrance. Based on the above reported results, our simulations suggest a possible role of residues Asp325 and Asp344 in tuning the pH-dependent catalytic activity of OGOX1. In order to give credit to such hypothesis, alanine mutagenesis experiments have been carried out as described in the next sections.

3.3. Heterologous expression of site directed OGOX1 variants

MD simulations identified two potential ionic bonds, i.e., Asp325-Arg327 and Asp344-Lys415, as responsible for modulating the size

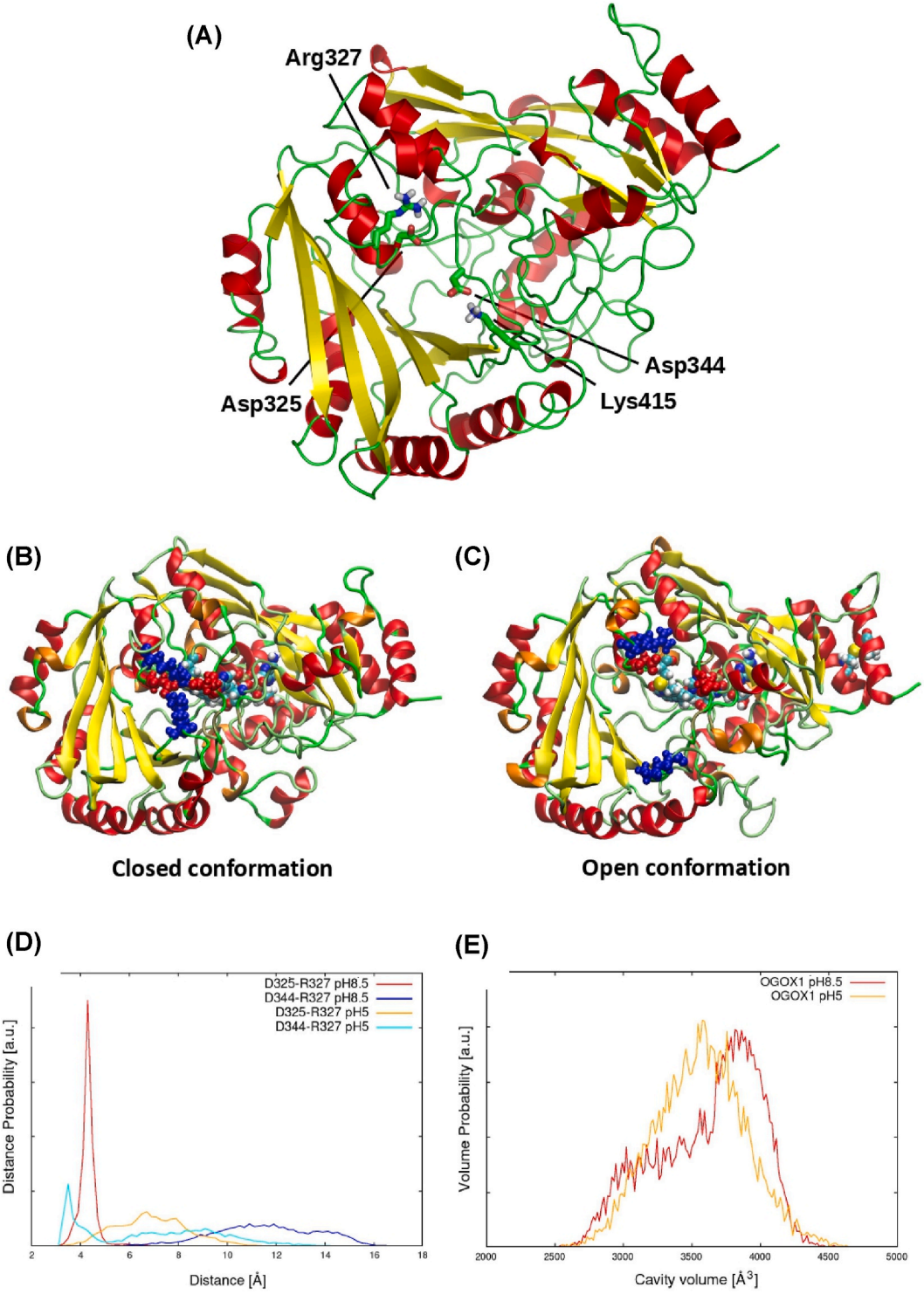

Fig. 3. Molecular dynamics analysis on OGOX1. (A) Cartoon representation of OGOX1 with Asp325, Arg327, Asp344, and Lys415 shown as sticks. (B) Representative structure of a closed conformation of the cavity. Asp325 and Asp344 (in red) and Arg327 and Lys415 (in blue) are shown as spheres. (C) Representative structure of an open conformation of the cavity. Asp325 and Asp344 (in red) and Arg327 and Lys415 (in blue) are shown as spheres. (D) The distribution of distances between Arg327 and the two aspartic acids Asp325 and Asp344 are reported for both the simulations. (E) The distribution of the cavity volume sampled along the two MD simulations is reported. (For interpretation of the references to color in this figure legend, the reader is referred to the Web version of this article.)

and flexibility of the enzyme cavity used to accommodate the OGs at pH 8.5. A multiple amino acid alignment between OGOX1 and other mature plant BBE-l enzymes indicated that the putative ionic bond formed by Asp325 and Arg327 is a specific feature of OGOX1 and OGOX2 (Fig. 4). It is worth noting that OGOX1 and OGOX2 were characterized by the highest pH-optimum of activity across the different BBE-l enzymes so far characterized (Benedetti et al., 2018; Locci et al., 2019; Toplak et al., 2018). This evidence strongly supported the involvement of the salt bridge Asp325-Arg327 in the increased activity of OGOX1 at alkaline condition. On the other hand, the putative salt bridge formed by Asp344 and Lys415 was shared by different BBE-l members including OGOX1, 3, 4 and CELLOX (Fig. 4).

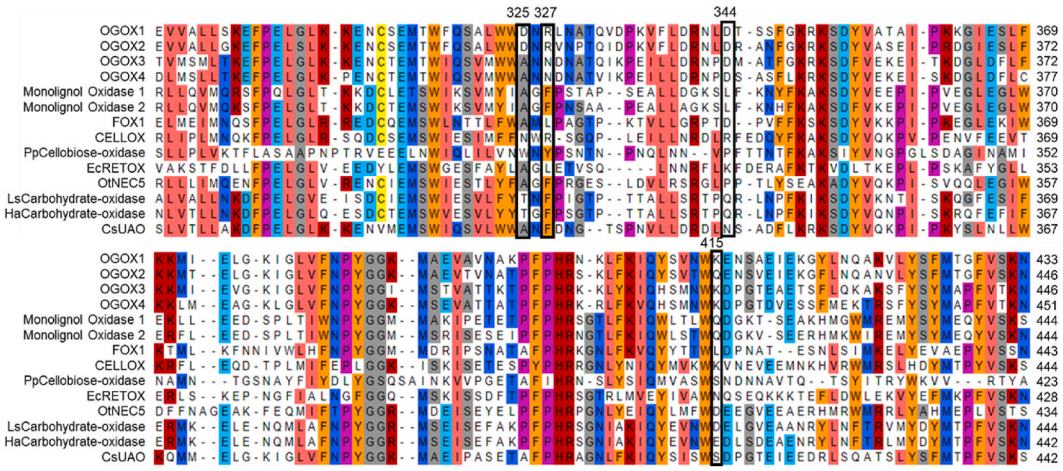

Fig. 4. Multiple amino acid alignment of the sequence of interest between mature OGOXs and other plant BBE-l proteins with known substrates. Identical colors refer to amino acids with identical/similar chemical properties that are conserved at least in 7 out 14 proteins. Numbering is from the first amino acid of each mature protein. Black boxes indicate the amino acid substitutions corresponding to the position D325, R327, D344 and K415 of OGOX1, putatively involved in the formation of stable salt bridges at alkaline pH condition [HaCarbohydrate-oxidase, Carbohydrate-oxidase from *Helianthus annuus*; LsCarbohydrate-oxidase, Carbohydrate-oxidase from *Lactuca sativa*; PpCellobiose-oxidase, Cellobiose-oxidase from *Physcomitrella patens*; OtNEC5, Nectarin V from Ornamental tobacco (*Nicotiana langsdorffii x N. sanderae*); EcRETOX, Reticuline Oxidase from *Eschscholzia californica*; CsUAO, Uronic Acid Oxidase from *Citrus sinensis*; CELLOX, BBE22 from *A. thaliana*; FOX1, BBE3 from *A. thaliana*; Monolignol Oxidase 1, BBE13 from *A. thaliana*; Monolignol Oxidase 2, BBE15 from *A. thaliana*; OGOX1, BBE20 from *A. thaliana*; OGOX2, BBE21 from *A. thaliana*; OGOX3, BBE2 from *A. thaliana*; OGOX4, BBE1 from *A. thaliana*]. (For interpretation of the references to color in this figure legend, the reader is referred to the Web version of this article.)

An MD-guided alanine mutagenesis approach was employed to confirm the involvement of the two ionic bonds in the pH dependent activity of OGOX1. Alanine scanning mutagenesis has been widely used in the past, allowing to identify the contribution of non-Ala amino acids (i) in the catalytic features of enzymes (Mitsuzawa et al., 2017), (ii) in the recognition specificities of enzyme-inhibitor interactions (Casasoli et al., 2009) as well as (iii) in protein function, stability and shape (Morrison and Weiss, 2001) since each Ala substitution examines the contribution of an individual amino acid sidechain to the functionality of the protein. In order to abolish the putative ionic bonds of pairs Asp325-Arg327 and Asp344-Lys415, we opted to mutagenize the negatively charged counterpart of each salt bridge (i.e., aspartic acid) into alanine because the latter residue naturally occurs at the corresponding position of other BBE-l enzymes (Fig. 4). Moreover, we also extended the alanine scanning mutagenesis to the cysteine residues C12 and C75 in order to investigate their potential role as regulative (as S-sulfidrilated residues) or structural determinants (as disulfide bridge) of H-OGOX1 (Fig. S4). Unfortunately, *P. pastoris* failed to express both H-OGOX1.C12A and H-OGOX1.C75A mutants indicating either that the alanine scanning mutagenesis was not the most appropriate method to get insights into their function or that these cysteines play a crucial role in the structural stability of the protein rather than in the regulation of enzymatic activity (Fig. 5A). The expression of H-OGOX1.D325A and H-OGOX1.D344A was successfully achieved in *P. pastoris* despite one of the mutants, i.e., H-OGOX1.D344A, was expressed at low level (Fig. 5A). After selecting the highest expressing transformants, both H-OGOX1. D325A and H-OGOX1.D344A were purified to homogeneity using the same procedure employed for H-OGOX1 (Fig. 5B). The expression yield of H-OGOX1.D325A and H-OGOX1.D344A was around 4 and 1 mg.L^{-1}, respectively.

3.4. Biochemical characterization of H-OGOX1 and site-directed variants H-OGOX1.D325A and H-OGOX1.D344A

The ABTS-HRP coupled assay was employed to characterize the activity of H-OGOX1 and of site-directed variants H-OGOX1.D325A and H-OGOX1.D344A at pH 5.0 and 8.5 by using OGs at concentrations ranging from 5 to 400 μM. The oxidase activity assay was conducted by coupling H_2O_2 production from OG oxidation to HRP mediated oxidation of ABTS into the cationic radical ABTS^{+}• (Baron et al., 1994) (Fig. 6A). The use of ABTS-HRP assay had two major advantages respect to the orange xylenol assay: (i) the ABTS-HRP assay results in a more accurate analysis since it can be measured in continuous whereas the orange xylenol method is an end-point assay, and (ii) the ABTS-HRP coupled assay may also reported.

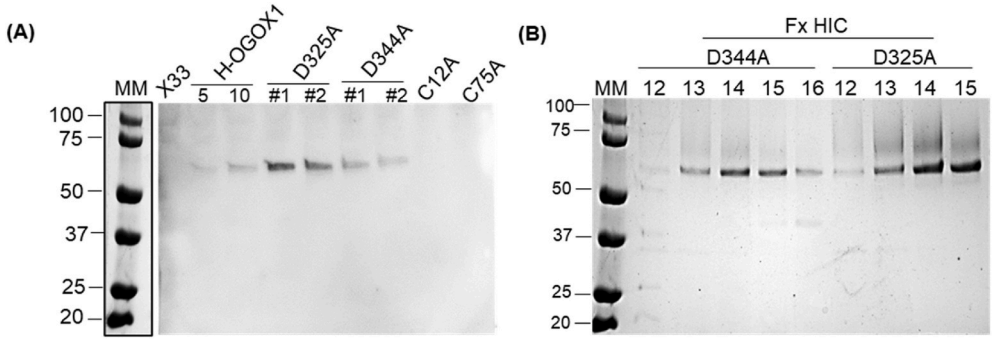

Fig. 5. Heterologous expression of H-OGOX1 mutants in *P. pastoris*. (A) Immunodecoration analysis of H-OGOX1 mutants Asp325A, Asp344A, Cys12A and Cys75A as detected in the culture filtrates from two independent *P. pastoris* transformants (#1–2) after 48h of methanol induction. 5 and 10 ng of pure H-OGOX1 and culture filtrate of wild-type *P. pastoris* (X33) were used as positive and negative control of enzyme expression, respectively. (B) SDS-PAGE/Coomassie blue staining analysis of H-OGOX1.D344A and H-OGOX1.D325A as detected in the fractions (Fx) eluted from the hydrophobic interaction chromatography (HIC). Molecular weight marker (MM) is

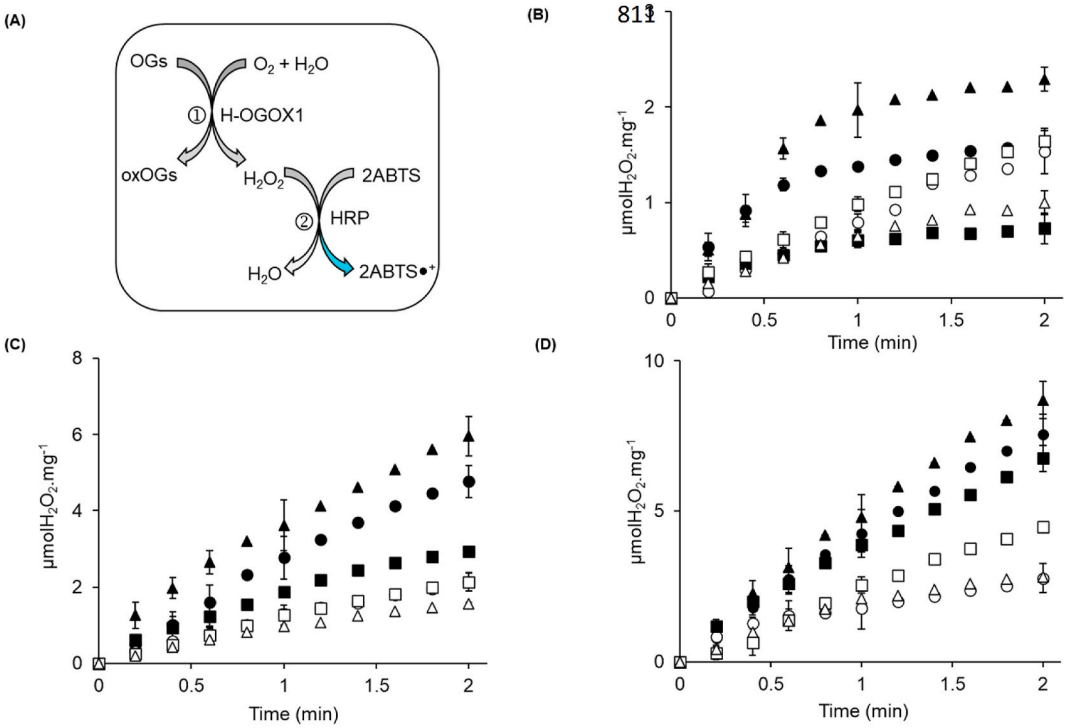

Fig. 6. Kinetic analysis of H-OGOX1 and site-directed mutants by the ABTS-HRP coupled assay. (A) Schematic representation of the two-step H-OGOX1/HRP-ABTS coupled assay used for kinetic measurements at pH 5.0 and 8.5. In step 1, H-OGOX1 oxidizes OGs by producing oxOGs and H_2O_2. In step 2, H_2O_2 is employed by HRP to oxidize ABTS (colourless) into the cation radical ABTS$\bullet^+$ (green colored). (B–D) OG-oxidizing activity of H-OGOX1 (circle), H-OGOX1.D325A (square) and H-OGOX1.D344A (triangle) as determined at pH 5.0 (white symbol) and 8.5 (black symbol) using 5 μM (B), 10 μM (C) and 40 μM (D) OGs as substrate. Values are mean ± SD (N = 3). For a clearer visualization, only some SD-error bars are reported. (For interpretation of the references to color in this figure legend, the reader is referred to the Web version of this article.)

preserve H-OGOX1 from the self-deleterious effects of H_2O_2-mediated oxidation since HRP exploits H_2O_2 released by OGOX1 to oxidize ABTS, thus lowering the amount of free H_2O_2 in the reaction mixture. Moreover, the k_{cat} values of HRP towards H_2O_2 and ABTS are higher than those of OGOX1 towards OGs (Humer and Spadiut, 2019), suggesting that OG- and ABTS-oxidation can proceed at the same rate at both the pH values (i.e., 5.0 and 8.5). It is worth noting that an HRP-based assay was recently employed also to determine the activity of fungal oligosaccharide oxidases (Haddad Momeni et al., 2021).

At acidic pH (5.0), H-OGOX1 was characterized by a K_M value of 4.6 ± 0.5 μM and a k_{cat} value of 93.5 ± 1.7 min^{-1}. At increasing pH (8.5), the K_M value was comparable to that observed at acidic pH whereas the k_{cat} value increased up to 213.5 ± 7.2 min^{-1}, indicating that the H-OGOX1 activity was boosted by alkaline pH up to 2.3-fold (Table 3). The mutation in H-OGOX1.D344A resulted in a slight increase in K_M at both pH values with respect to H-OGOX1, and in a k_{cat} value of 276.3 ± 9.5 min^{-1} at pH 8.5, indicating that the H-OGOX1.D344A activity was boosted by alkaline pH up to 3.2-fold (Table 3). On the other hand, the mutation Asp325Ala gave the major effect on the kinetic constants of H-OGOX1; K_M value of H-OGOX1.D325A increased at both acidic and alkaline pH values by 3.5- and 9.3-fold, respectively, indicating a reduced affinity for the substrate whereas k_{cat} was slightly increased; this behavior is likely induced to the acquired capacity of the mutant enzyme to detach from the substrate more easily, as indicated by its higher K_M, thus increasing turn-over (Table 3). H-OGOX1.D325A showed the lowest increase of activity from acidic to alkaline pH since its activity showed only a 1.6-fold enhancement (Table 3).

Table 3
Kinetic parameters of H-OGOX1 and site-directed mutants by the ABTS-HRP coupled assay. Values of K_M (μM), V_{max} (μmol H_2O_2.mg^{-1}.min^{-1}) and k_{cat} (min^{-1}) as determined at pH 5.0 and 8.5 using OGs at a concentration ranging from 5 to 400 μM.

Parameter	H-OGOX1		H-OGOX1.D325A		H-OGOX1.D344A	
pH	5.0	8.5	5.0	8.5	5.0	8.5
K_M	4.6 ± 0.5	4.5 ± 0.8	16.0 ± 1.3	42.2 ± 2.6	10.6 ± 0.6	9.2 ± 1.2
V_{max}	1.60 ± 0.03	3.6 ± 0.1	2.9 ± 0.1	4.6 ± 0.1	1.6 ± 0.03	4.7 ± 1.2
k_{cat}	93.5 ± 1.7	213.5 ± 7.2	168.7 ± 0.1	271.6 ± 4.9	93.3 ± 2.0	276.3 ± 9.5
k_{cat}/K_M	20.3	47.4	10.5	6.4	9.4	30.0
k_{cat} pH 8.5/5.0	2.3		1.6		3.2	

All these results taken together indicated subtle differences between the kinetic constants of the three OGOX1 isoforms at the steady state conditions, indicating that both mutations did not completely disrupt enzyme function. However, the OGs concentration used for the steady-state analysis especially at high concentrations is not reliable under physiological conditions; as a matter of fact, the concentration of OGs used to trigger the defense responses in plants usually ranged from 4 to 40 μM (Galletti et al., 2008; Gravino et al., 2015), suggesting that the biologically active concentration of OGs within the plant tissue is presumably lower. By measuring the μmoles of H_2O_2 generated per mg of H-OGOX1 over time, it was evident that at lower (and physiologically active) OG concentration, Asp325 and Asp344 acted in antagonistic manner in modulating the activity of OGOX1 at pH 8.5 but not at pH 5.0 (Fig. 6B–D). Compared to the wild-type enzyme, Asp344Ala mutation increased OGOX1 activity whereas the Asp325Ala mutation reduced it, suggesting that pH dependent activity of OGOX1 may be dependent on the antagonistic action of both amino acids at alkaline pH (Fig. 6B–D). The kinetic analysis also revealed that at low OG concentration (i.e., 5 μM) the activity of H-OGOX1.D325A was lower at pH 8.5 than at pH 5.0 (Fig. 6B), due to a marked reduction in the affinity towards OGs in alkaline condition (Table 3). Accordingly, the initial velocity V_0 values

of the enzymatic reactions shown in Fig. 6B–D confirmed this trend of activity as a peculiar characteristic of H-OGOX1.D325A (Table 4).

The pH-dependent activity of H-OGOX1 and site-directed variants was then investigated by the orange-xylenol assay (Fig. 7). Here, the orange-xylenol assay was used in replacement of the ABTS-HRP coupled assay since HRP is unstable at pH values higher than 9.0 (https://www.sigmaaldrich.com/deepweb/assets/sigmaaldrich/product/documents/254/641/p8375dat.pdf). However, it is worth considering that the activity of OGOXs in the orange-xylenol assay, differently from the ABTS-HRP coupled assay (Fig. 6A), is affected by the same H_2O_2 generated upon OG-oxidation (Fig. S1). In accordance with the previous analysis (Fig. 6D, Table 3), the ratio between the relative activities at pH (9.0/5.0) was lower for H-OGOX1.D325A (i.e., 3.8; calculated as 55.2%: 14.6%) than for H-OGOX1 (i.e., 5.7; calculated as 92.9%: 16.3%), whereas H-OGOX1.D344A showed the highest ratio between the two relative activities (i.e., 7.8; calculated as 82.2%: 10.5%) (Fig. 7); thus, the tendency of H-OGOX1.D325A was dependent on its K_M that, differently from that of H-OGOX1 and H-OGOX1.D344A, strongly reduced the enzyme affinity for OGs at alkaline pH condition (Table 3). On the other hand, the activity of H-OGOX1.D344A mutant was characterized by the highest increase passing from acid to alkaline pH (Figs. 6D and 7). In conclusion, under physiologically active OG concentration, the mutations Asp325Ala and Asp344Ala made the pH-dependent activity of OGOX1 less and more sensitive to alkaline pH changes, respectively, without any significant change in its pH-optimum (Fig. 7).

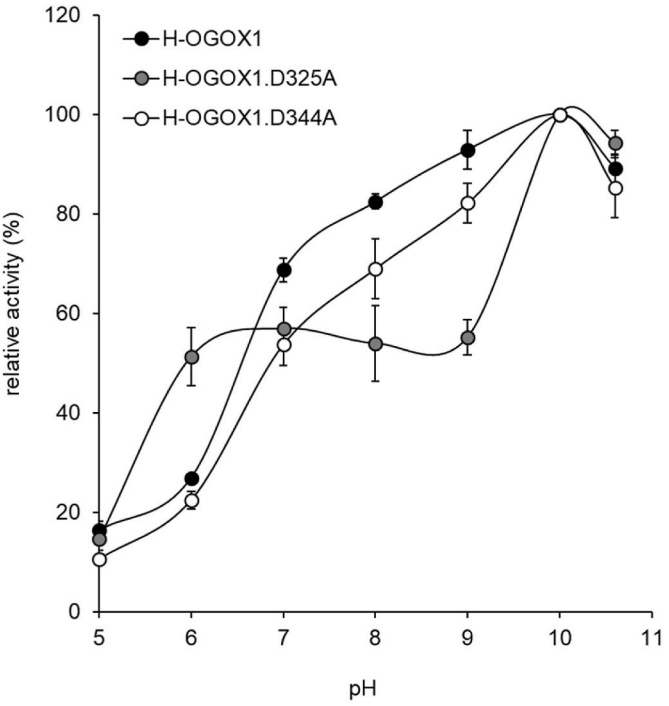

Fig. 7. pH-dependent activity of H-OGOX1 and site-directed mutants by the orange-xylenol assay. Effect of pH on the activity of H-OGOX1, H-OGOX1.D325A and H-OGOX1.D344A expressed as relative activity (%) using 40 μM OGs as substrate. Values are mean ± SD (N = 4).

4. Discussion

In this work, MD was successfully employed to identify two amino acid pairs, i.e., Asp325-Arg327 and Asp344-Lys415, involved in the pH dependent activity of OGOX1. In particular, the residues Asp325 and Asp344 were demonstrated to be involved in the pH dependent activity of OGOX1, likely due to the formation of two distinct salt bridges on the edge of enzyme cavity at alkaline conditions (pH 8.5). As verified by functional studies, the mutation of Asp325 and Asp344 significantly affects the catalytic properties of OGOX1. The simulations suggest that the perturbation of the salt bridges affects the catalytic activity in the same way as the pH does. Asp325Ala mutation, as well as low pH condition, would prevent the formation of any salt bridge, thus leading to a less active form of the enzyme. Conversely, Asp344Ala mutation does not have an analogue in pH tuning, nevertheless, our simulations show that Asp344 salt bridge may have a correlation with the volume of the cavity leading to the active site. However, as observed in the low pH dynamics, the catalytic properties of OGOX1 are not only defined by the size of the cavity, but also by its flexibility. The higher flexibility of the protein region between residue 430 and residue 455, as found in the low pH simulation, corresponds to a reorientation of Tyr451 with respect to the starting structure. It was suggested that Tyr479 in Monolignol Oxidase 2 (corresponding to Tyr451 in OGOX1) stabilizes the deprotonated state of Tyr193 (Tyr166 in OGOX1) by hydrogen bonding, thus enabling the deprotonation of the substrate (Daniel et al., 2015). The conformation of Tyr193 found in the X-ray structure of Monolignol Oxidase 2 was kept in our high pH simulation, while it was lost along the low pH simulation, possibly contributing to the reduced catalytic activity of OGOX1 found at low pH. The amino acid alignment between OGOX1 and other plant BBE-l enzymes (Fig. 4) indicated that the salt bridge formed by Asp325 and Arg327 is a specific determinant of OGOX1 and OGOX2, i.e., the OGOX enzymes showing the highest activity at alkaline pH. According to our results, the introduction of a salt bridge formed by Asp325 and Arg327 in the corresponding amino acid sites of OGOX3 and OGOX4 isoforms may on one side modulate the activity of these enzymes at increasing pH (Fig. 7), and on the other increase their affinity towards OGs (Table 3). From an evolutionary perspective, the advantage of evolving several OGOX members with different OG affinities and the role of amino acid Asp325 in such sub-functionalization remains unclear. Interestingly, several mutations in Monolignol Oxidase 2 produced a small increase in the pH-optimum of activity of the enzyme (Messenlehner et al., 2021); in this regard, it would be interesting to evaluate whether such mutations, once introduced in our OGOX1 mutants, may result in a synergistic effect (Table 5).

The use of an ABTS-HRP coupled assay allowed to achieve more

Table 4
Values of initial velocity (V_0) of H-OGOX1 and site-directed mutants by the ABTS-HRP coupled assay. Values of V_0 (μmol H_2O_2.mg^{-1}.min^{-1}) as obtained from the reactions shown in Fig. 6B–D. Values are mean ± SD (N = 3).

OG (μM)	H-OGOX1		H-OGOX1.D325A		H-OGOX1.D344A	
5	0.8 ± 0.1	1.9 ± 0.1	0.8 ± 0.1	0.6 ± 0.1	0.4 ± 0.1	1.9 ± 0.1
10	1.1 ± 0.1	2.6 ± 0.3	1.2 ± 0.1	1.6 ± 0.3	0.7 ± 0.1	2.5 ± 0.1
40	1.4 ± 0.2	3.5 ± 0.3	2.1 ± 0.2	2.9 ± 0.5	1.3 ± 0.1	3.9 ± 0.3
pH	5.0	8.5	5.0	8.5	5.0	8.5

Table 5
Mutations increasing the pH-optimum of activity of Monolignol Oxidase 2 (MLO2) towards more alkaline values and the corresponding amino acid residues in OGOX1.

MLO2	OGOX1
R292M	R265
Q438V	Q409
Y479F	Y451
Y117F	Y92
N411V	N383
K436L	K407
Y193F	Y166

precise and reliable analysis over time, compared to the previous characterization of OGOX1 as obtained by the "orange-xylenol" end-point method (Benedetti et al., 2018). H-OGOX1 was characterized by a higher k_{cat} value, i.e., 213.5 min^{-1} *vs* 131.6 min^{-1} (the latter value calculated as $k_{catpH11}$ * $R.A._{pH8.5}$), and a lower K_M, i.e., 4.6 μM *vs* 8 μM, highlighting the contribution of the expression strategy, purification procedure and enzyme assay in the enzyme characterization of recombinant enzymes.

Interestingly, the high amino acid identity between the four OGOX members from *A. thaliana* and Uronic Acid Oxidase from *Citrus sinensis* (CsUAO) (Fig. S7) suggested that CsUAO may be another BBE-l enzyme with OG-oxidizing activity (Wei et al., 2020). Accordingly, the K_M of UAO towards D-galacturonic acid, i.e., 3.9 mM, is about 848-fold higher than those displayed by OGOX1 towards OGs, i.e., 4.6 μM (Table 3), indicating that D-galacturonic acid could not be the preferred substrate for CsUAO. Interestingly, CsUAO is characterized by Ala and Phe residues at the corresponding positions 325–327 of OGOX1 (Fig. 4) that in turn could be mutagenized in Asp-Arg residues in order to create a salt bridge and increase its affinity towards OGs (Wei et al., 2020).

OxOGs lose their nature of DAMPs and acquire an increased resistance to enzymatic hydrolysis by fungal polygalacturonases (PGs), preventing a direct release of D-galacturonic acid from oxOGs (Fig. 1) (Benedetti et al., 2018). Thus, the kinetic parameters of the specific couple PG-OGOX under investigation as well as their relative concentration will determine the fate of D-galacturonic acid residue at the reducing end of each OG (hydrolysis *vs* oxidation). Intriguingly, the apoplastic alkalinization during pathogenesis may favor the production of oxOG (i.e., oxidation) rather than the hydrolysis of D-galacturonic acid since k_{cat} of OGOX1 increases at alkaline pH, i.e., from 93.5 to 213.5 min^{-1} (Table 3) whereas k_{cat} of microbial PGs decreases since PGs are generally characterized by a lower range of pH-optimum of activity (3–6). Under this perspective, the amino acid residues that contribute to the pH dependent activity of OGOX enzymes play a primary role in plant protection. Intriguingly, Asp and Arg residues could be introduced by site-directed mutagenesis in the corresponding position 325–327 of other plant BBE-l enzymes (Fig. 4) as well as fungal oligosaccharide oxidases, in order to improve their pH-dependent activity at alkaline pH values comprised between 8 and 10. In turn, should these substitutions successfully affect the pH dependent activity of other oligosaccharide oxidases, these mutated enzymes could be used in industrial applications as Lytic Polysaccharide Monooxygenase (LPMO)-boosting enzymes (Haddad Momeni et al., 2021), allowing to perform lytic-oxidative reactions on lignocellulose at more alkaline pH ranges.

Author contributions

B.M. and D.N. conceived the project. A.S., B.M. and M.B. designed the experiments, A.S. performed the experiments and analyzed the data jointly with B.M, M.B and F.A. V.S. and M.G. contributed to design and perform the experiments. M.C., D.N., M.F. and L.G. performed molecular dynamics analysis and analyzed data jointly with B.M., M.B. and F.A. A. S., D.N., M.B. and M.C. wrote the manuscript draft whereas B.M., M.B. and F.A. edited the final version of the manuscript. B.M. and M.B. supervised the research. All authors have approved the final manuscript.

Declaration of competing interest

The authors declare that they have no known competing financial interests or personal relationships that could have appeared to influence the work reported in this paper.

Acknowledgements

The authors gratefully acknowledge Prof. Felice Cervone, Prof. Giulia De Lorenzo and Dr. Daniela Pontiggia (Dept. of Biology and Biotechnology "C. Darwin", University of Rome, Sapienza) for providing OGs, and Prof. Giuseppina Pitari (Dept. of Life, Health and Environmental Sciences, University of L'Aquila) for inspiring discussions on flavoenzymes.

Appendix A. Supplementary data

Supplementary data to this article can be found online at https://doi.org/10.1016/j.plaphy.2021.11.011.

Funding

This work was supported by the Italian Ministry of University and Research (MIUR) under grant PON for industrial research and experimental development ARS01_00881 and under grant PRIN 2017ZBBYNC, both funded to Prof. Benedetta Mattei.

References

Abraham, M., Murtola, T., Schulz, R., Páll, S., Smith, J., Hess, B., Lindahl, E., 2015. GROMACS: high performance molecular simulations through multi-level parallelism from laptops to supercomputers. SoftwareX 1–2, 19–25. https://doi.org/10.1016/j.softx.2015.06.001.

Almagro Armenteros, J., Tsirigos, K., Sønderby, C., Petersen, T., Winther, O., Brunak, S., Nielsen, H., 2019. SignalP 5.0 improves signal peptide predictions using deep neural networks. Nat. Biotechnol. 37 (4) https://doi.org/10.1038/s41587-019-0036-z.

Baron, A., Stevens, C., Wilmot, C., Seneviratne, K., Blakeley, V., Dooley, D., McPherson, M., 1994. Structure and mechanism of galactose oxidase. The free radical site. J. Biol. Chem. 269 (40).

Bayly, C., Cieplak, P., Cornell, W., Kollman, P., 1993. A well-behaved electrostatic potential based method using charge restraints for deriving atomic charges: the RESP model. J. Phys. Chem. 97 https://doi.org/10.1021/j100142a004.

Benedetti, M., Locci, F., Gramegna, G., Sestili, F., Savatin, D., 2019. Green production and biotechnological applications of cell wall lytic enzymes [review]. Appl. Sci. 9 (23), 5012. https://doi.org/10.3390/app9235012.

Benedetti, M., Mattei, B., Pontiggia, D., Salvi, G., Savatin, D.V., Ferrari, S., 2017. Methods of isolation and characterization of oligogalacturonide elicitors. Methods Mol. Biol. 1578, 25–38 (IN FILE).

Benedetti, M., Verrascina, I., Pontiggia, D., Locci, F., Mattei, B., De Lorenzo, G., Cervone, F., 2018. Four Arabidopsis berberine bridge enzyme-like proteins are specific oxidases that inactivate the elicitor-active oligogalacturonides. Plant J. : Cell Mol. Biol. 94 (2) https://doi.org/10.1111/tpj.13852.

Berendsen, H., Postma, J., van Gunsteren, F., DiNola, A., Haak, J., 1984. Molecular dynamics with coupling to an external bath [research-article]. J. Chem. Phys. 81, 3684–3690. https://doi.org/10.1063/1.448118.

Biasini, M., Bienert, S., Waterhouse, A., Arnold, K., Studer, G., Schmidt, T., Schwede, T., 2014. SWISS-MODEL: modelling protein tertiary and quaternary structure using evolutionary information. Nucleic Acids Res. 42, W252–W258. Web Server issue.

Borner, G.H.H., Sherrier, D.J., Weimar, T., Michaelson, L.V., Hawkins, N.D., Macaskill, A., Dupree, P., 2005. Analysis of detergent-resistant membranes in Arabidopsis. Evidence for plasma membrane lipid rafts. Plant Physiol. 137 (1), 104–116.

Bussi, G., Donadio, D., Parrinello, M., 2007. Canonical sampling through velocity rescaling. J. Chem. Phys. 126 (1) https://doi.org/10.1063/1.2408420.

Cai, H., Liu, X., Zou, J., Xiao, J., Yuan, B., Li, F., Cheng, Q., 2018. Multi-wavelength spectrophotometric determination of hydrogen peroxide in water with peroxidase-catalyzed oxidation of ABTS. Chemosphere 193. https://doi.org/10.1016/j.chemosphere.2017.11.091.

Casasoli, M., Federici, L., Spinelli, F., Di Matteo, A., Vella, N., Scaloni, F., De Lorenzo, G., 2009. Integration of evolutionary and desolvation energy analysis identifies functional sites in a plant immunity protein. Proc. Natl. Acad. Sci. U.S.A. 106 (18), 7666–7671. https://doi.org/10.1073/pnas.0812625106.

Daniel, B., Konrad, B., Toplak, M., Lahham, M., Messenlehner, J., Winkler, A., Macheroux, P., 2017. The family of berberine bridge enzyme-like enzymes: a treasure-trove of oxidative reactions. Arch. Biochem. Biophys. 632, 88–103. https://doi.org/10.1016/j.abb.2017.06.023.

Daniel, B., Pavkov-Keller, T., Steiner, B., Dordic, A., Gutmann, A., Nidetzky, B., Macheroux, P., 2015. Oxidation of monolignols by members of the berberine-bridge enzyme family suggests a role in plant cell wall metabolism. J. Biol. Chem. 290 (30), 18770–18781. https://doi.org/10.1074/jbc.M115.659631.

Daniel, B., Wallner, S., Steiner, B., Oberdorfer, G., Kumar, P., van der Graaff, E., Macheroux, P., 2016. Structure of a berberine bridge enzyme-like enzyme with an active site specific to the plant family brassicaceae. PLoS One 11 (6), e0156892. https://doi.org/10.1371/journal.pone.0156892.

Elortza, F., Mohammed, S., Bunkenborg, J., Foster, L.J., Nuhse, T.S., Brodbeck, U., Jensen, O.N., 2006. Modification-specific proteomics of plasma membrane proteins: identification and characterization of glycosylphosphatidylinositol-anchored proteins released upon phospholipase D treatment. J. Proteome Res. 5 (4), 935–943.

Essmann, U., Perera, L., Berkowitz, M., Darden, T., Lee, H., Pedersen, L., 1998. A smooth particle mesh Ewald method. J. Chem. Phys. 103, 8577–8592. https://doi.org/10.1063/1.470117.

Felle, H.H., 2001. pH: signal and messenger in plant cells. Plant Biol (Stuttg) 3 (6), 577–591. https://doi.org/10.1055/s-2001-19372.
Frisch, M.J., Trucks, G.W., Schlegel, H.B., Scuseria, G.E., Robb, M.A., Cheeseman, J.R., Fox, D.J.G., 2016. Gaussian 16 rev. C.01. Inc. https://gaussian.com/relnotes/.
Galletti, R., Denoux, C., Gambetta, S., Dewdney, J., Ausubel, F.M., De Lorenzo, G., Ferrari, S., 2008. The AtrbohD-mediated oxidative burst elicited by oligogalacturonides in Arabidopsis is dispensable for the activation of defense responses effective against *Botrytis cinerea*. Plant Physiol. 148 (3), 1695–1706. https://doi.org/10.1104/pp.108.127845 (NOT IN FILE).
Gravino, M., Savatin, D.V., Macone, A., De Lorenzo, G., 2015. Ethylene production in *Botrytis cinerea*- and oligogalacturonide-induced immunity requires calcium-dependent protein kinases. Plant J. 84 (6), 1073–1086. https://doi.org/10.1111/tpj.13057.
Haddad Momeni, M., Fredslund, F., Bissaro, B., Raji, O., Vuong, T., Meier, S., Abou Hachem, M., 2021. Discovery of fungal oligosaccharide-oxidising flavo-enzymes with previously unknown substrates, redox-activity profiles and interplay with LPMOs. Nat. Commun. 12 (1) https://doi.org/10.1038/s41467-021-22372-0.
Haruta, M., Sabat, G., Stecker, K., Minkoff, B., Sussman, M., 2014. A peptide hormone and its receptor protein kinase regulate plant cell expansion. Science (New York, N. Y.), 6169. https://doi.org/10.1126/science.1244454, 343.
Hess, B., Bekker, H., Berendsen, H., Fraaije, J., 1997. LINCS: a linear constraint solver for molecular simulations. J. Comput. Chem. 18 (12), 1463–1472. https://doi.org/10.1002/(SICI)1096-987X(199709)18:12<1463::AID-JCC4>3.0.CO;2-H.
Hou, S., Liu, Z., Shen, H., Wu, D., 2019. Damage-associated molecular pattern-triggered immunity in plants. Front. Plant Sci. 10, 646. https://doi.org/10.3389/fpls.2019.00646.
Humer, D., Spadiut, O., 2019. Improving the performance of horseradish peroxidase by site-directed mutagenesis. Int. J. Mol. Sci. 20 (4) https://doi.org/10.3390/ijms20040916.
Humphrey, W., Dalke, A., Schulten, K., 1996. VMD: visual molecular dynamics. J. Mol. Graph. 14 (1) https://doi.org/10.1016/0263-7855(96)00018-5.
Jorgensen, W.L., Chandrasekhar, J., Madura, J.D., 1983. Comparison of simple potential functions for simulating liquid water. J. Chem. Phys. 79, 926. https://doi.org/10.1063/1.445869.
Klarzynski, O., Plesse, B., Joubert, J.M., Yvin, J.C., Kopp, M., Kloareg, B., Fritig, B., 2000. Linear beta-1,3 glucans are elicitors of defense responses in tobacco. Plant Physiol. 124 (3), 1027–1038.
Laurent, B., Chavent, M., Cragnolini, T., Dahl, A., Pasquali, S., Derreumaux, P., Baaden, M., 2015. Epock: rapid analysis of protein pocket dynamics. Bioinformatics 31 (9). https://doi.org/10.1093/bioinformatics/btu822.
Li, H., Robertson, A., Jensen, J., 2005. Very fast empirical prediction and rationalization of protein pKa values. Proteins 61 (4). https://doi.org/10.1002/prot.20660.
Locci, F., Benedetti, M., Pontiggia, D., Citterico, M., Caprari, C., Mattei, B., De Lorenzo, G., 2019. An Arabidopsis berberine bridge enzyme-like protein specifically oxidizes cellulose oligomers and plays a role in immunity. Plant J. 98 (3), 540–554. https://doi.org/10.1111/tpj.14237.
Maier, J., Martinez, C., Kasavajhala, K., Wickstrom, L., Hauser, K., Simmerling, C., 2015. ff14SB: improving the accuracy of protein side chain and backbone parameters from ff99SB. J. Chem. Theor. Comput. 11 (8) https://doi.org/10.1021/acs.jctc.5b00255.
Mattei, B., Spinelli, F., Pontiggia, D., De Lorenzo, G., 2016. Comprehensive analysis of the membrane phosphoproteome regulated by oligogalacturonides in *Arabidopsis thaliana*. Front. Plant Sci. 7, 1107. https://doi.org/10.3389/fpls.2016.01107.
McNicholas, S., Potterton, E., Wilson, K.S., Noble, M.E., 2011. Presenting your structures: the CCP4mg molecular-graphics software. Acta Crystallogr D Biol Crystallogr 67 (Pt 4), 386–394. https://doi.org/10.1107/S0907444911007281 (NOT IN FILE).
Messenlehner, J., Hetman, M., Tripp, A., Wallner, S., Macheroux, P., Gruber, K., Daniel, B., 2021. The catalytic machinery of the FAD-dependent AtBBE-like protein 15 for alcohol oxidation: Y193 and Y479 form a catalytic base, Q438 and R292 an alkoxide binding site. Arch. Biochem. Biophys. 700, 108766 https://doi.org/10.1016/j.abb.2021.108766.
Mitsuzawa, S., Fukuura, M., Shinkawa, S., Kimura, K., Furuta, T., 2017. Alanine substitution in cellobiohydrolase provides new insights into substrate threading. Sci. Rep. 7 (1) https://doi.org/10.1038/s41598-017-16434-x.
Moroz, N., Huffaker, A., Tanaka, K., 2017. Extracellular alkalinization assay for the detection of early defense response. Current Protocols Plant Biol. 2 (3) https://doi.org/10.1002/cppb.20057.
Morrison, K., Weiss, G., 2001. Combinatorial alanine-scanning. Curr. Opin. Chem. Biol. 5 (3) https://doi.org/10.1016/s1367-5931(00)00206-4.
Nuhse, T.S., Bottrill, A.R., Jones, A.M., Peck, S.C., 2007. Quantitative phosphoproteomic analysis of plasma membrane proteins reveals regulatory mechanisms of plant innate immune responses. Plant J. 51 (5), 931–940.
Pontiggia, D., Benedetti, M., Costantini, S., De Lorenzo, G., Cervone, F., 2020. Dampening the DAMPs: how plants maintain the homeostasis of cell wall molecular patterns and avoid hyper-immunity. Front. Plant Sci. 11, 613259 https://doi.org/10.3389/fpls.2020.613259.
Puigbò, P., Guzmán, E., Romeu, A., Garcia-Vallvé, S., 2007. OPTIMIZER: a web server for optimizing the codon usage of DNA sequences. Nucleic Acids Res. 35 https://doi.org/10.1093/nar/gkm219. Web Server issue.
Páll, S., Abraham, M., Kutzner, C., Hess, B., Lindahl, E., 2015. Tackling exascale software challenges in molecular dynamics simulations with GROMACS. *Solving software Challenges for exascale*. https://doi.org/10.1007/978-3-319-15976-8_1.
Toplak, M., Wiedemann, G., Ulicevic, J., Daniel, B., Hoernstein, S.N.W., Kothe, J., Macheroux, P., 2018. The single berberine bridge enzyme homolog of *Physcomitrella patens* is a cellobiose oxidase. FEBS J. 285 (10), 1923–1943. https://doi.org/10.1111/febs.14458.
Wang, J., Wolf, R., Caldwell, J., Kollman, P., Case, D., 2004. Development and testing of a general amber force field. J. Comput. Chem. 25 (9) https://doi.org/10.1002/jcc.20035.
Wei, Y., Tan, Y., Ang, E., Zhao, H., 2020. Identification and characterization of Citrus peel uronic acid oxidase. Chembiochem : Euro. J. Chem. Biol. 21 (6) https://doi.org/10.1002/cbic.201900546.
Wu, S.X., Letchworth, G.J., 2004. High efficiency transformation by electroporation of *Pichia pastoris* pretreated with lithium acetate and dithiothreitol. Biotechniques 36 (1), 152–154.
Zafred, D., Steiner, B., Teufelberger, A.R., Hromic, A., Karplus, P.A., Schofield, C.J., Macheroux, P., 2015. Rationally engineered flavin-dependent oxidase reveals steric control of dioxygen reduction. FEBS J. 282 (16), 3060–3074. https://doi.org/10.1111/febs.13212.